CHALMERS
UNIVERSITY OF TECHNOLOGY

Road Surface Characterization Using a 77-81 GHz Polarimetric Radar

Citation for the original published paper (version of record):
Vassilev, V. (2024). Road Surface Characterization Using a 77-81 GHz Polarimetric Radar. IEEE Transactions on Intelligent Transportation Systems, 25(9): 12829-12834.
http://dx.doi.org/10.1109/TITS.2024.3360702

Road surface characterization using a 77-81 GHz polarimetric radar

Vessen Vassilev

***Abstract*—Various road surfaces are studied through monostatic polarimetric-radar measurements at 77-81 GHz in real traffic conditions. Dry asphalt of different roughness is compared to wet asphalt and gravel in terms of their entropy and the balance between surface, volume and double bounce scattering. It is shown that asphalt surfaces of different roughness are distinguishable. Wet surface is clearly detectable through its reduced entropy, a result of enhanced surface scattering. Measurements of pavement and gravel surfaces are also presented and compared to asphalt. The ultimate goal of this study is to relate friction to the polarimetric parameters measured in real time while the vehicle is in motion. Ice and snow covered road surfaces are of particular interest, but are not covered in this paper.**

***Index Terms*—Radar polarimetry, Ice, road surface identification, target entropy**

I. Introduction

A sensor capable of analysing properties of the road surface in front of a moving vehicle can assist the driver or the control system of the car in detecting sections of the road with reduced friction. Of particular interest are formations such as thin (black) ice, which are indistinguishable visually. Mm-wavelengths (30-300 GHz) are attractive for traffic safety related applications due to their short wavelengths, which allow building compact antennas in combination with availability of technology and frequency spectrum. Mm-wave radars are already commonly used in modern cars to analyse the traffic surrounding and can potentially be adapted to distinguish between dry/icy or wet road surfaces.

A method of surface classification is presented in [1] where a bistatic radar at 20-24 GHz is used to collect and analyse polarimetric data from surfaces of different roughness. The polarimetric scattering matrix is analysed using Stokes parameters to extract information about the surface properties.

Previous studies to detect ice formations on road surfaces include a 61 GHz bistatic polarimetric radar sensor capable of distinguishing various types of surfaces under a moving vehicle as presented in [2], and a 24 GHz monostatic sensor [3], [4] both measuring backscattering coefficients for vertical, horizontal and cross polarizations.

Modeling and measurements at 94 GHz of the dielectric constant and polarimetric backscatter responses of dry, ice and water covered asphalt surfaces are presented in [5], [6].

In the studies above, the surfaces are characterized through their polarimetric backscatter coefficients or their ratios and thus do not consider the random nature of the road surfaces as distributed target.

V. Vassilev is with the Department of Microtechnology and Nano Science at Chalmers University of Technology and VVWaves AB, Sweden

Manuscript received August 2023; revised November, 2023.

For a sensor mounted on a moving vehicle every measurement is performed on a different section of the surface. Due to the random nature of road surfaces a single measurement is not sufficient to extract reliable information about the properties of the surface. Therefore, a statistical approach has to be adopted. Such a method has been developed for synthetic aperture radar (SAR) observations [7] and has been used to classify surfaces of various types: identify frozen areas [8] and measure roughness of road surfaces from airborne observations [9].

To analyse the surfaces, in this work we use polarimetric attributes such as target entropy (TE), which is a measure of target disorder, and the balance between surface/volume scattering (also called auxiliary angle).

In our previous work [10] it was shown that polarimetric attributes such as entropy and polarimetric pedestal can be used to detect whether a surface is dry, wet or ice covered. A laboratory network analyser was used to perform a number of monostatic measurements in W-band (75-110 GHz), on a surface in different states and in controlled laboratory environment. The polarimetric attributes are derived from the eigenvalues of the averaged coherence/covariance matrix. It was shown that ice covered surface features higher entropy, while wet surface shows decreased entropy compared to the surface in dry condition.

A similar work is presented in [11] where entropy, auxiliary angle α and anisotropy are used to identify the road surface condition. The auxiliary angle contains additional information not present in the entropy and thus helps resolve surfaces of different properties, but with similar entropy.

To be able to measure the polarimetric attributes of road surfaces from a vehicle in motion and in real time, we developed a compact polarimetric FMCW radar based on a commercial chipset for the 77-81 GHz band. We used the radar to collect data from typical road surfaces in real traffic conditions. Dry asphalt of different roughness, gravel, pavement and wet asphalt surface are measured and mapped through their entropy and auxiliary angle α. So far icy and snow covered surfaces are not characterized in real traffic, however the ultimate goal of this work is to relate the polarimetric attributes of various surfaces to their friction properties, and possibly detect extreme low-friction conditions such ”black ice”.

This manuscript is organised as follows. Section II presents the method of calculating the polarimetric attributes. A brief description of radar sensor is presented in section III. The results of the measurements are found in IV where the surfaces are compared in terms of their entropy and the dominant scattering mechanism (the Auxiliary angle α). This section also presents details on the measurement procedure and a few

examples of irregularities on the surfaces and how they inevitably affect the polarimetric attributes. Section V discusses how surfaces that produce similar polarimetric attributes can be distinguished.

The measurement results are summarized in section VI together with some conclusions on the identifiability of the surfaces.

II. Method

Even though asphalt is a surface with uniform properties, it represents a random distributed target and can exhibit large variations from one illumination area to another. A statistical approach is needed in order to extract useful information about the properties of the surface. Target entropy (TE) and auxiliary angle α [7] are two polarimetric attributes, which are calculated after decomposition of the coherence matrix.

The input for the calculation of the coherence matrix is the measured scattering matrix, which is defined as:

$$\begin{bmatrix} S_{VV} & S_{VH} \\ S_{HV} & S_{HH} \end{bmatrix} \tag{1}$$

Where the first index indicates the polarization of the transmitter and the second the polarization orientation of the receiver. The reciprocity theorem of backscattering states that $S_{HV} = S_{VH}$ [12]. The coherence matrix *T* can be represented as the product of the coherence vector k with its transposed complex conjugate [7] and contains *3x3* elements:

$$T = kk^{\dagger} \tag{2}$$

where the coherence vector k is given by:

$$k = \begin{bmatrix} S_{HH} + S_{VV} \\ S_{HH} - S_{VV} \\ 2S_{HV} \end{bmatrix} \tag{3}$$

To calculate the eigenvalues and eigenvectors of the coherence matrix a minimum of 3 measurements are needed. For a set of N number of measurements, the measurement matrix M consists of N columns of the measured coherence vector in the presence of noise.

$$M = \begin{bmatrix} | & | & .. & | \\ k^1 & k^2 & .. & k^N \\ | & | & .. & | \end{bmatrix} \tag{4}$$

The coherence matrix $\hat{T}$ is obtained by multiplying the measurement M matrix with its transposed complex conjugate (denoted as †) and dividing by the number of measurements.

$$\hat{T} = \frac{MM^{\dagger}}{N} \tag{5}$$

The coherence matrix can be represented through its eigenvalues and eigenvectors.

$$\hat{T} = \lambda_1 \left[e_1.e_1^{\dagger}\right] + \lambda_2 \left[e_2.e_2^{\dagger}\right] + \lambda_3 \left[e_3.e_3^{\dagger}\right] \tag{6}$$

Where e_i are the 3 elements column eigen-vectors and λ_i are the corresponding eigenvalues.

A. Entropy

Entropy is a measure of the randomness of the scattering process and has a value of 0 for a single non-random target and 1 for a highly random distributed target where several scattering mechanisms are involved. After decomposition of the coherence matrix, as shown in eq. (6) the entropy is calculated from the 3 eigenvalues [7] as shown in eq. (7) and (8).

$$H = -\sum_{i=1}^{3} P_i . \log_3(P_i) \tag{7}$$

where Pi has a meaning of probability and represents the relative importance of the corresponding eigenvalue with respect to the total scattered power. P_i is given by:

$$P_i = \frac{\lambda_i}{\lambda_1 + \lambda_2 + \lambda_3} \tag{8}$$

The physical interpretation of the eigenvalues can be found in [13] and suggests that $\lambda 3$ depends on the cross polarization return, which associates this eigenvalue with diffuse scattering. Scattering resulting from odd and even number of reflections is represented by $\lambda 1$ and $\lambda 2$, respectively.

B. Auxiliary angle α

To characterize the surfaces the α-Entropy space, as described in [7] can be used. The mean polarimetric scattering angle α is one of the parameters defining the orientation of a polarization ellipse in the H/V plane. It is calculated, as shown in eq. (9), from the first element of each of the eigenvectors from eq. (6).

$$\alpha = \sum_{i=1}^{3} P_i . acos(|e_{i1}|) \tag{9}$$

In the context of polarimetric measurements α indicates the dominant scattering mechanism as follows:

- α = 0^0 surface scattering only
- α = 45^0 dipole/volume scattering
- α = 90^0 double bounce scattering

It should be considered that α and entropy are not independent as they are both related to the probabilities from eq. 8. The region of possible α values in the following figures is confined by the dotted lines.

III. Polarimetric radar

The radar sensor, shown in Fig. 1, is based on AWR 1843 chipset from TI, it uses 2 transmitters and 2 receivers to measure the [S] scattering matrix (1). A conical horn antenna is followed by a waveguide polarization filter, which separate/combine the H and V components into orthogonal rectangular waveguides connected to the corresponding transmitter/receiver.

The horn antenna is integrated with a Teflon lens, the output beam-waist of the horn and the lens is located at 50 cm from the aperture, with a beam-waist diameter of 47 mm.

The [S] matrix is measured in two frames: in the first frame the H transmitter is active and in the second the V, H and V

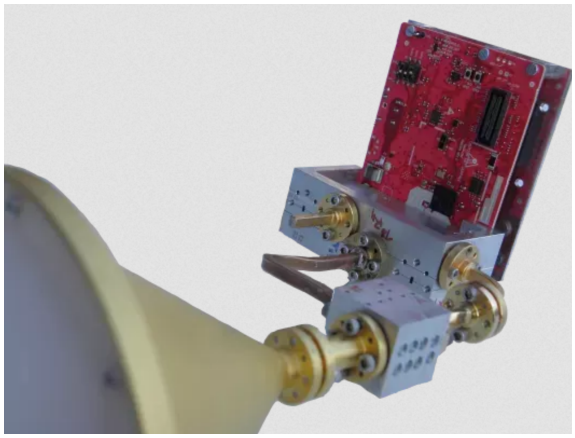

Fig. 1. A picture of the polarimetric radar sensor.

TABLE I
FRAME CONFIGURATION

Number of frames	Samples in 1 frame	Sampling freq, MHz	Time/ frame, us	Slope MHz/usec	BW GHz	Max Range, m
2	64	5	46	140	1.8	4.2

receivers are receiving in both frames. The frame configuration is summarized in Table I. The radar board sends data to a computer through a UART interface, where a python script performs the estimation of the polarimetric attributes in real time.

When pointed to a spherical calibration target the cross-pol component S_{HV} is 20 dB lower than the co-pol components S_{HH} and S_{VV}. This cross-pol component is contributed by the hardware and in particular in the horn/lens as measurements of the polarization filter shows polarization isolation better than -37dB across the band. The response of each transmitter/receiver combination is calibrated using the same spherical calibration target. The co-pol components are aligned in magnitude and range, while the cross-pol component is aligned only in range.

IV. MEASUREMENTS

A dedicated firmware was constructed that can handle polarimetric measurements in real time. However, the firmware of the radar is constructed in a way that can not handle phase offsets due to Doppler effect. Therefore, to avoid phase offsets between frames due to motion, the radar is looking sideways at a distance of about 2.3m from the surface as shown in Fig. 2.

As seen from Table I it takes 2 frames of 46 us to measure the [S] matrix (1), which is sent to a computer every 25 ms.

A video camera takes images to relate the radar measurements to the type of the surface under test. During the measurements the car is moving at a speed in the range of 25-50km/h. The speed does not affect the measurement, but at speeds below a certain threshold the entropy starts to drop because the surface is not sampled independently. This speed depends on the size of the radar beam at the plane where it meets the surface. Fig. 2 illustrates the measurement setup and the beam size and location. The beam intersection with the surface at a range of 2.3 m is an ellipse with major/minor diameters of 232/176 mm. Fig. 3 shows a picture of the radar mounted on the vehicle.

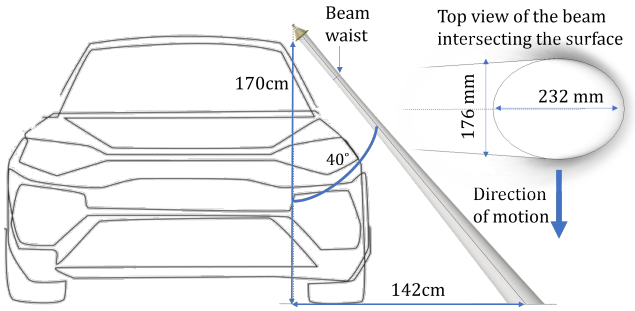

Fig. 2. Illustration of the radar placement and its beam geometry. The insert shows the cross section of the beam with the surface.

Fig. 3. The radar mounted on a vehicle.

An example of the magnitudes of the 3 scattering parameters is shown in Fig. 4 for the case of a dry asphalt surface. The response from surface is visible at ranges from 2.1 to 2.4m.

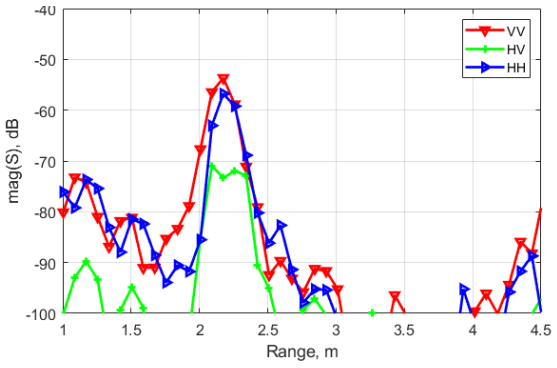

Fig. 4. Magnitude of scattering parameters of 1 frame. The surface covers range from 2.1 to 2.4 m.

The entropy and α are then calculated for each range cell. A sequence of measured entropy averaged over the range where the surface is visible is shown in Fig. 5. In this measurement

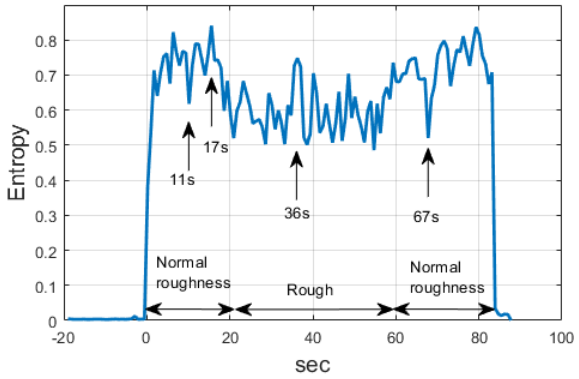

Fig. 5. Transition from dry asphalt of normal roughness to rough and back to normal again.

the vehicle is transiting from a surface with normal roughness to a rough surface (at around 18s after start) and back to a section of normal roughness (at 58s after start). The rougher section of the surface shows reduced entropy. This is expected observation as the higher roughness enhances the surface reflection, so the dominant surface-scattering becomes even higher. From Fig. 5 it is obvious that the measured entropy features large variations. These variations in most cases can be associated with structures on the road surface. Since we use a video camera to film the surface, some of the entropy variations from Fig. 5 are identified with the images shown in Fig. 6. The drop in entropy at 11s after the start is due to a water drainage structure where the grooves of the metal cover on top of the catch basin enhance the dominant surface scattering resulting in drop of the entropy. The peaks at 17s and 36s are result of the radar beam pointing to road marking lines. These lines are much smoother than the asphalt resulting in decreased surface reflection and enhanced volume and double bounce scatterings in other words increased entropy. The entropy drop at 67s is associated with a patched area on the surface. It is not clear how this particular patch influences the balance between the surface scattering and volume scattering, but the effect of it is still measurable.

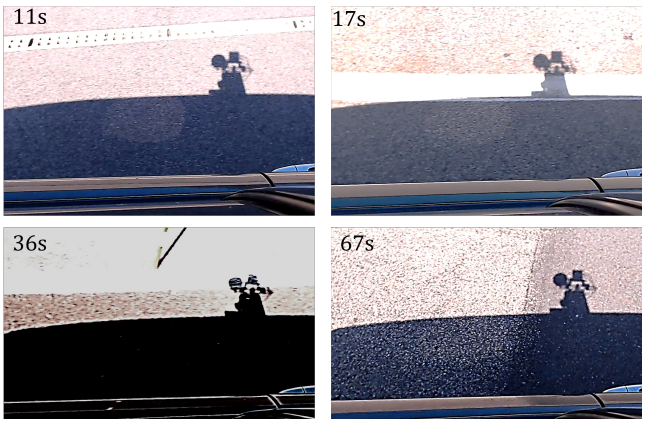

Fig. 6. Examples of some of the irregularities responsible for the variations of the entropy from Fig. 5 including: metal cover, marking lines and patches.

In real measurement scenario these irregularities will exist, therefore in the following measurements they are not filtered resulting in spread of the values of the measured α and entropy.

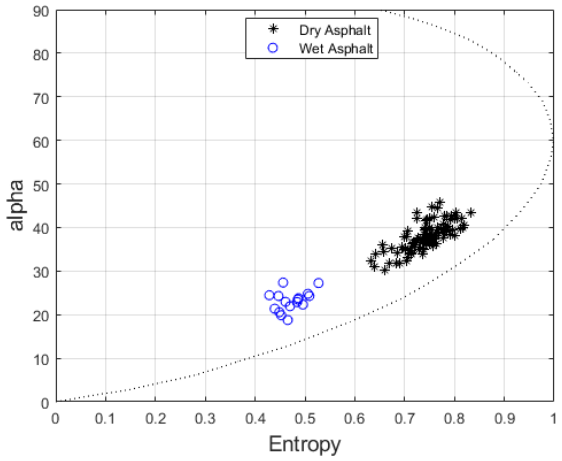

Fig. 7. Asphalt of normal roughness in dry and wet condition. The dry surface is measured over a 99s interval, the wet surface patch is measured over 16s.

A. Asphalt surface dry and wet

In this section an asphalt surface of normal roughness is measured in dry state and after spraying a thin layer of water over a certain area of the surface. Fig. 7 compares the result on an α-Entropy plot as explained in section II. Presence of water on the surface enhances the surface reflection, which makes the dominant surface scattering even stronger, resulting in reduced entropy and α value. The clouds of ponts are well separated and identifiable.

B. Dry asphalt surfaces of different roughness

In this section we compare 3 dry asphalt surfaces of different roughness to see how the surface roughness affects the polarimetric parameters.

- Normal: this is a surface with roughness, which is typical for the majority of public roads. We assume surface, RMS value $\approx$ 0.9mm.
- Rough: we do not know the value of roughness for this surface but it appears unusually rough which is not found normally on public roads. We assume this surface has been treated with Asphalt Removal Cold Milling Machine and its roughness is expected to be in the range of 3-6 mm.
- Smooth, that would be typical for new asphalt surface.

We can observe that rough surface has less entropy, while smooth surface features higher entropy. This is expected as surface-scattering dominate in all surfaces. Rougher surface has higher surface reflection, so the dominant scattering is further enhanced by the increased roughness moving the rough surface towards less entropy and lower α. Smooth asphalt, on the other hand, has less contribution from surface scattering and thus higher levels of volume and dihedral scattering, resulting in higher entropy and α values.

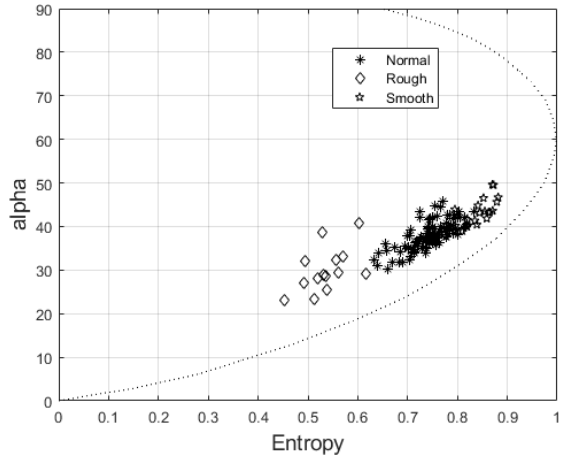

Fig. 8. α, entropy plot for dry surfaces of different roughness

C. Gravel

A section of a gravel surface is measured and compared to a dry asphalt of normal roughness as shown in in Fig. 9. The gravel shows higher entropy and α compared to asphalt of normal roughness, but there is a considerable overlap between the 2 "clouds". The centre of the gravel cloud sits in between the normal and smooth asphalt surfaces. The spread of the points results in considerable overlap between these 3 surfaces and their identification will require additional processing steps, which are discussed in the following section.

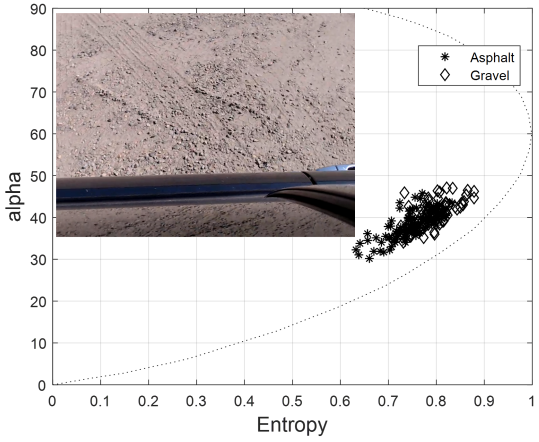

Fig. 9. Gravel and asphalt of normal roughness.

TABLE II
MEAN VALUE AND STANDARD DEVIATION OF ENTROPY AND α FOR 40 FRAMES (1S).

Surface Condition	Asphalt Rough	Asphalt Normal	Asphalt Smooth	Asphalt Normal Wet	Gravel	Pavement
$\overline{Entropy}$	0.54	0.74	0.84	0.47	0.8	0.58
$\sigma(Entropy)$	.043	0.04	.031	.031	.036	.014
$\overline{\alpha}$	30	38	43	23.1	41	27.8
$\sigma(\alpha)$	5.1	3.2	3.2	2.37	3.1	1.65

D. Pavement

A section of pavement shown in Fig. 10 was measured and compared to asphalt. The pavement shows reduced entropy and α compared to the surrounding asphalt surface and.

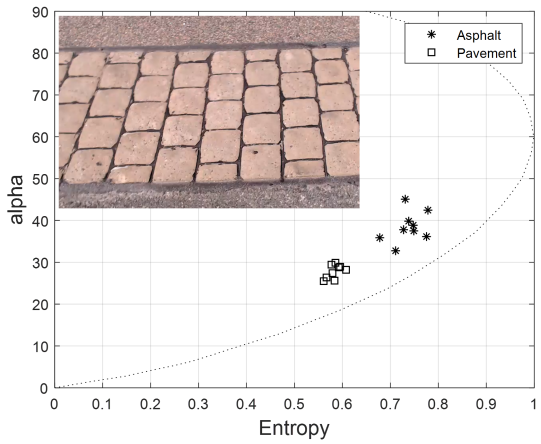

Fig. 10. Pavement and asphalt of normal roughness measured over 9s interval each.

A summary of the measured expected values and standard deviation of entropy and α are summarized in Table II.

V. RESOLVING SURFACES WITH SIMILAR ENTROPY AND α

We have seen from the previous section that some surfaces produce similar α/entropy values, as in the case of gravel and asphalt, from Fig. 9. The probability density functions (PDFs) of these 2 surfaces are shown in Fig. 11 for the same data as presented in Fig. 9.

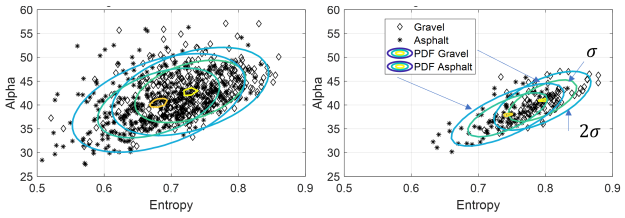

Fig. 11. α, entropy plot of gravel and asphalt and their corresponding PDFs. To the left: 10 frames (0.25s), to the right 40 frames (1s) per measurement. The contours in the PDF are located at σ and 2σ.

Obviously increasing the number of frames used for the estimation of α/entropy helps reduce the variance in the measurement and reduces the region of overlapping between the 2 PDFs. However, any remaining points falling in the region of PDF overlap are ambiguous and can not be used for identifying the surfaces. These points can be excluded through the likelihood ratio test [14].

In this test the following binary classification problem can be defined: a measurement belongs to surface (a) or surface (b). If the PDFs of each surface are known, the likelihood of a measurement to belong to surface (a) or (b) can be calculated. For example, to identify a point to a surface (a) the likelihood (a) evaluated at a point (entropy,α) needs to be higher than the likelihood (b), evaluated at the same point, by a certain factor

called likelihood ratio (LR). If a measurement does not fulfil the condition of belonging to group (a) or (b) it is considered as ambiguous and is removed. To compute the PDFs of the surfaces, the asphalt/gravel measurements displayed in Fig. 11 are used as a training sequence.

After obtaining the two PDF through measurement of known surfaces (training data set), the likelihood ratio test is performed on a second data set containing both asphalt and gravel (not the same surfaces as from Fig. 11). The data set before and after applying the likelihood ratio test is shown in Fig. 12 where it can be seen that the points that do not "pass" the LR condition are filtered out. The higher the LR is selected the more confidence there will be in assigning a measurement point to its corresponding surface. However, some points at the extreme of the clouds are still erroneously classified. To eliminate these remaining 'false alarms' the measurement time needs to be increased.

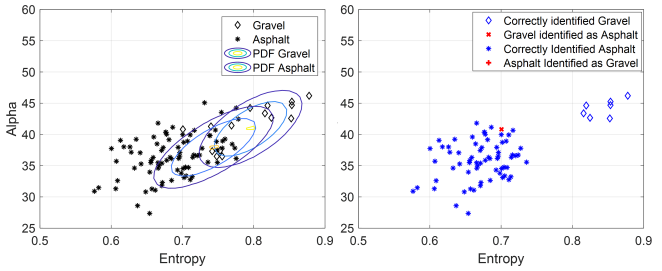

Fig. 12. α, entropy plot of a second set of gravel/asphalt measurement. The figure to the left shows the raw data together with the PDFs from the training sequence in Fig. 11. To the right is the points after applying the likelihood ratio test. One gravel measurement point, marked with (x) is erroneously identified as asphalt. The likelihood ratio for this test is 3.

VI. Conclusion

This work addresses the feasibility of using polarimetric radar sensor mounted on a vehicle in motion to characterize properties of road surfaces relevant to traffic safety. Different surfaces are measured and characterized in terms of their entropy and dominant scattering mechanism (auxiliary angle α). Each surface produces a cloud of points on the 2-D α entropy plot. The spread of the cloud to a large extend is due to irregularities present on the surface, such as marking lines, patches, cracks etc. Other contributions for the variations might be lying under the surface. For the measurements presented in section IV the irregularities causing spread in the values of α/entropy have not been filtered. One way to make the cloud points more "compact" is to increase in the number of measurements used in the α/entropy estimation. In the results from Fig. 7 to Fig. 9 a set of 40 measurements of the [S]-matrix are used in the α/entropy estimation. With 25ms to measure the [S]-matrix, the α/entropy values are updated each second.

Rough asphalt features lower entropy and larger surface scatter contribution (lower α) while smooth surface behaves in the opposite direction: higher entropy larger volume scatter contribution (higher α value). The 3 dry asphalt surfaces of different roughness are distinguishable in Fig. 8 with some points overlapping at the edges of the clouds.

Wet asphalt of normal roughness is clearly distinguishable from dry asphalt of the same roughness with good separation between the clouds (Fig. 7). However, rough asphalt and wet asphalt of normal roughness are not separated so well and there is an overlap between the clouds (see Fig. 7, 8) possibly due to irregularities in both surfaces as discussed in section IV. Even though we do not know the value of roughness, it should be pointed out that the rough surface is of rather high roughness, which is not found normally on public roads.

Gravel has higher entropy and α compared to dry asphalt of normal roughness but their typical values are close and there is a considerable overlap between the "clouds" of gravel and rough/smooth surfaces as seen in Fig. 8 and 9. Similarly, pavement is sitting close to rough asphalt. To help distinguish such surfaces, the following measures can be applied: increase the number of frames for the calculation of the coherence matrix, apply likelihood ratio test, use additional data from other types of sensors to help eliminate the remaining ambiguous points.

Acknowledgment

This work was partly financed by Sweden's innovation agency Vinnova within the program "Strategic vehicle research and innovation". Currently it is supported by the "GigaHertz-ChaseOn Bridge center" at Chalmers. The hardware used for the measurements is provided by VVWaves AB, Sweden.

References

[1] H. Rudolf, G. Wanielik, A.J. Sieber, "Road condition recognition using microwaves", *Proceedings of Conference on Intelligent Transportation Systems*, Nov. 1997.

[2] N. Kees, J. Detlefsen, "Road surface classification by using a polarimetric coherent radar module at millimeter waves", *IEEE MTT-S International Microwave Symposium Digest*, May 1994.

[3] V. Viikari, "Road-Condition Recognition Using 24-GHz Automotive Radar", *IEEE Transactions on Intelligent Transportation Systems, Vol. 10, No. 4*, December 2009.

[4] J. Häkli et al., "Road surface condition detection using 24 GHz automotive radar technology," *in Proc. 14th Int. Radar Symp. (IRS)*, vol. 2, Jun. 2013, pp. 702–707.

[5] K. Sarabandi, E. S. Li and A. Nashashibi, "Modeling and measurements of scattering from road surfaces at millimeter-wave frequencies," *IEEE Transactions on Antennas and Propagation*, vol. 45, no. 11, pp. 1679-1688, Nov. 1997.

[6] E. S. Li and K. Sarabandi, "Low grazing incidence millimeter-wave scattering models and measurements for various road surfaces", *IEEE Transactions on Antennas and Propagation*, vol. 47, no. 5, pp. 851-861, May 1999.

[7] S. H. Cloude, "An Entropy Based Classification Scheme for Land Applications of Polarimetric SAR", *IIEEE Transactions on Geoscience and Remote Sensing*, (vol. 35), Jan. 1997.

[8] T. Jagdhuber, et. al, "Identification of Soil Freezing and Thawing States Using SAR Polarimetry at C-Band", *Remote Sens.* 2014.

[9] A. Babu, S. Baumgartner,"Road Surface Quality Assessment Using Polarimetric Airborne SAR", *IEEE Radar Conference*, Sept. 2020.

[10] V. Vassilev, "Road surface recognition at mm-wavelengths using a polarimetric radar", *IEEE Transactions on Inteligent Transportation Systems*,Vol. 23, Issue: 7, July 2022.

[11] W. Bouwmeester, F. Fioranelli and A. G. Yarovoy, " Road Surface Conditions Identification via H α A Decomposition and its Application to mm-Wave Automotive Radar", *IEEE Transactions on Radar Systems*, Vol. 1, 2023.

[12] Tsang L., et. al., "Theory of Microwave Remote Sensing", *Wiley and Sons*, April 1985.

[13] Ulaby, "Microwave radar and radiometric remote sensing", *The University of Michigan Press*, 2014.

[14] U. Spagnolini, "Statistical Signal Processing in Engineering", Ch. 23 Classification and Clustering, *John Wiley and Sons Inc.*, 2018.

Vessen Vassilev received M.Sc. degree in radio communications from Sofia Technical University, Sofia, Bulgaria, in 1995, and M.Sc. degree in digital communications from Chalmers university of technology, Gothenburg, Sweden, in 1998. In 2003 he received a Ph.D. degree from the department of radio and space science at Chalmers. From 1998 to 2008, he was involved in the development of cryogenic millimeter-wave receivers for applications in radio astronomy and space sciences. Instruments designed by him have been in operation at the Atacama Pathfinder Experiment (APEX) Telescope in Chile and Onsala Space Observatory in Sweden. Since 2008, he is with the microwave electronics laboratory, department of microtechnology and nanoscience at Chalmers. His current research interests include the development of millimeter-wavelength sensors based on monolithic microwave integrated circuit technologies.